Available online at www.sciencedirect.com

ScienceDirect

Procedia Engineering 191 (2017) 689 – 696

Procedia Engineering

www.elsevier.com/locate/procedia

Symposium of the International Society for Rock Mechanics

Visualization of the Evolution of the Fracture Process Zone in Sandstone by Transmission Computed Radiography

Leona Vavro[a,*], Kamil Souček[a], Daniel Kytýř[b], Tomáš Fíla[b], Zbyněk Keršner[c], Martin Vavro[a]

[a]*Institute of Geonics of the CAS, Studentská 1768, 708 00 Ostrava-Poruba, Czech Republic*
[b]*Institute of Theoretical and Applied Mechanics of the CAS, Prosecká 809/76, 190 00 Prague 9, Czech Republic*
[c]*Brno University of Technology, Faculty of Civil Engineering, Veveří 331/95, 602 00 Brno, Czech Republic*

Abstract

The article deals with the use of computed X-ray radiography to visualize the development of the fracture process zone in the rock samples. For radiographic observations during the three-point bending loading, glauconitic sandstone from the Řeka quarry (sometimes also referred to as Godula sandstone) was used. The chevron-notched cylindrical specimens with the diameter of 29 mm and 120 mm nominal length were prepared from the sandstone blocks. These specimens were subjected to the Chevron Bend (CB) test carried out in accordance with the ISRM suggested methodology; the span was 94 mm. The evolution of the fracture process zone was continuously scanned using X-ray radiography during the realized Mode I fracture toughness tests (FTT). The scanning was conducted using an industrial X-ray micro-tomographic inspection system equipped with a flat panel X-ray detector of 4,000 × 4,000 pixels and micro-focus X-ray source with reflection target, which are very suitable for obtaining highly detailed radiographic images during the FTT tests. Three-point bending tests were carried out using an in-house designed table-top loading device, construction of which allows precise control of the loading during testing. Continuous X-ray examination and subsequent radiographic image analysis enable investigation of the crack initiation and the process zone development during FTT and represents a useful tool for a better understanding of failure behavior of the rock material during the loading process.

Peer-review under responsibility of the organizing committee of EUROCK 2017

Keywords: Fracture process zone; fracture toughness; Chevron Bend (CB) test; glauconitic sandstone; X-ray radiography

* Corresponding author. Tel.: +420-596-979-239; fax: +420-596-979-452.
E-mail address: leona.vavro@ugn.cas.cz

Peer-review under responsibility of the organizing committee of EUROCK 2017
doi:10.1016/j.proeng.2017.05.233

1. Introduction

The process of crack formation in quasi-brittle materials leads to the damage of the material and to energy consumption in the direct proximity of the crack, i.e. in the fracture process zone (FPZ). The shape of the fracture process zone during the crack growth varies, and simultaneously the consumption of energy needed for crack propagation changes. The damage area in quasi-brittle materials macroscopically differs from the plastic zone developing at the crack tip in ductile materials (e.g. metals) [1]. Advanced computational tools to analyze fracture behavior of elements and structures of quasi-brittle materials (cement composites, concrete) have recently been created [2]. The FPZ in concrete is currently being studied using experimental techniques, such as high speed photography, acoustic emission testing, scanning electron microscopy (SEM) and laser-speckle interferometry [3]. Numerous numerical analyses of FPZ in concrete specimens have also been performed in this scientific field.

The research in fracture behavior of rocks and analyses of the scope and shape of the FPZ in rock materials builds on the advances of all the above mentioned studies and techniques and, therefore, is based on the advanced theories of damage of these quasi-brittle materials. So far, FPZs in rocks have been investigated experimentally and numerically in a number of studies. Experiments were performed on various types of test specimens and using different types of tests, in particular SCB (Semi-Circular Bend test) [4], CCNBD (Crack Chevron Notched Brazilian Disc test) [5], and three point bending test [1, 6]. In connection with the size effect, the FPZ was also analyzed using the method of acoustic emissions [1, 4], or laser speckle interferometry [7]. As in the case of other quasi-brittle materials, many numerical studies [1, 6] and mathematical models revealing regularities of the development of FPZ of rocks were made. Also, fracture behavior of rocks at static and various cyclic loadings was observed [5]. After the tests, X-ray computed micro-tomography (X-ray CT) was applied. The finding that fracture bifurcation is significantly higher during cyclic loading of the sample is one of the basic outputs of that research. From this point of view, the X-ray CT as well as computed radiography represent a novel and useful laboratory technique allowing for 3D visualization and analysis of FPZ in different types of materials [8].

This article presents experimental monitoring of the development of the FPZ in glauconitic sandstone using radiography imaging during the Chevron Bend (CB) fracture toughness test (FTT). The whole process of FPZ evolution until specimen rupture was on-line recorded and subsequently compared with the obtained load–displacement diagrams. The X-Ray CT scanning of tested samples during selected FTT tests was performed too, but due to the sample size it was not possible to reconstruct the CT volume for successful subsequent image analysis of FPZ development. The main advantage of the X-ray radiography, as well as the X-ray CT is, in particular, the possibility of spatial analysis of the FPZ development.

2. Experiment setup

2.1. Test specimen and rock material

Cylindrical CB specimens (29 mm in diameter, 120 mm in length) were drilled from a sandstone block in the laboratory. The core drilling was carried out parallel to the bedding planes. In the middle of the test specimen the chevron edge notch using a circular diamond blade was cut (Fig. 1). The width of the chevron notch was 1.4 mm.

The glauconitic sandstones from the Řeka quarry (Moravian-Silesian Beskids Mountains, approx. 30 km NE from the city of Ostrava, Czech Republic) have been deliberately selected for this study. These greenish so-called Godula sandstones are mainly formed by quartz grains (ca 40–60 % of the whole rock volume); feldspars grains (ca 7–15 % vol.) and mica flakes (ca 5 % vol., muscovite > biotite) occur less frequently. The average grain size of the quartz fragments ranged from 0.18 mm to 0.39 mm. Lithic clasts (5–20 %) are represented mainly by fine-grained quartzite with similar grain sizes to the quartz grains. In some samples, the microfossils are relatively common. A clay matrix (10–20 %) is formed by dominant illite. Small, sub-rounded to rounded green-colored pellets of authigenic glauconite (up to 0.7 mm, 1–5 % vol.) occur frequently. Rock cement includes early diagenetic quartz, a very variable content of authigenic calcite and dolomite, and traces of fine-grained pyrite. Rock texture is psammitic, sub-angular, and poorly sorted, with long (flattened) to partly sutured grain contacts (for more detail, see [9]). Basic physical and mechanical properties of the Godula sandstones are shown in Table 1.

Table 1. Selected material properties of glauconitic sandstones from the Řeka quarry [9, 10].

Parameter	Average value	Min. – max. values	Number of tested samples
Bulk density [kg/m^3]	2.489	2.274 – 2.612	72
Water absorption capacity by weight [%]	2.1	0.7 – 3.0	12
Ultrasonic wave velocity [m/s]	3.710	3.120 – 4.290	89
Uniaxial compressive strength (dry sample) [MPa]	126.2	102.7 – 155.8	53
Young's modulus (dry sample) [MPa]	19.680	18.400 – 27.600	10
Poisson's ratio (dry sample) [–]	0.20	0.10 – 0.25	5
Flexural strength (dry sample) [MPa]	11.9	9.7 – 14.0	9
Splitting tensile strength (dry sample) [MPa]	5.67	4.00 – 10.00	12

Fig. 1. Test specimen for CB fracture toughness test (before testing – *left*, after testing – *right*).

2.2. Table-top loading device

The specimens were subjected to a three-point bending test using a custom design loading device (Fig. 2A). The device was designed particularly for in-situ mechanical testing in X-ray scanners. The deforming structure of the materials in the loading device is simultaneously observed using X-ray radiography and/or X-ray tomography that allows for identification of structural changes in the specimen and for an advanced analysis of the deformation behavior (e. g. identification of the fracture process zone in a quasi-brittle material [8]). The specimen is placed in the loading chamber (Fig. 2B) that is made of a thin-walled (0.6 mm) high-strength carbon fiber composite with very low attenuation of X-rays. The loading chamber is connected with the rest of the device by a rigid bayonet lock made of high-performance aluminum alloy. The loading part of the device is located in the aluminum frame above the loading chamber and contains a loading mechanism (stepper motor, zero-backlash harmonic drive and high-precision ball screw), load-cell with 2 kN loading capacity, and loading platen. The bending supports are made of a cylindrical carbon fiber composite with diameter 10 mm. This configuration shows low attenuation of X-rays and allows for distortion-free X-ray imaging in the vicinity of the bending support. Movement precision of the loading mechanism is 5 μm and the experiments are controlled using computer numerical control (CNC) software.

In the bending tests the loading device and X-ray radiography were used to observe the structural damage in the vicinity of the chevron notch, and to analyze the fracture process zone in the Godula sandstone specimens. The experiments were carried out as displacement-driven with loading rates of 5, 1 and 0.5 μm/s, respectively. The distance of the lower supports was set to 94 mm. The specimens were subjected to a three-point bending at constant loading rate from the initial contact up for quasi-brittle failure of the material.

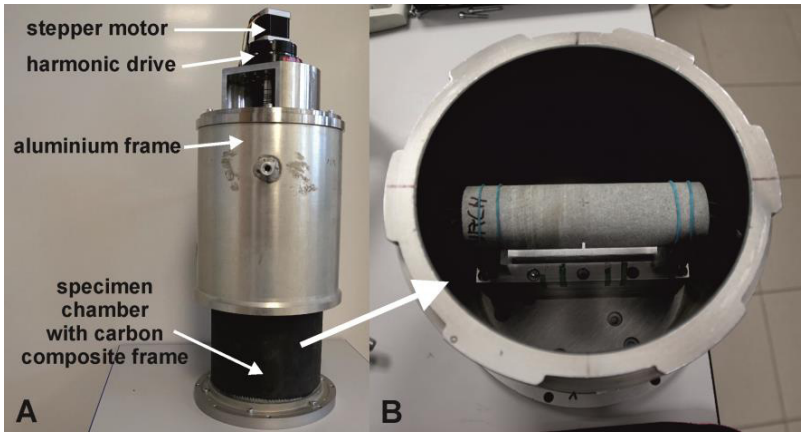

Fig. 2. The loading device (A – general view, B – view into the specimen chamber with a test sample).

2.3. X-ray CT scanner

For the investigations of the process zone evolution during FTT, an X-ray micro-CT scanner XT H 225 ST (Nikon Metrology NV) was used. It is a fully automated apparatus equipped with a rotary stage and advanced control system supporting tomography and radiography imaging. Table 2 outlines the basic technical parameters of the apparatus. This device was used in the mode to obtain radiographic images during FTT only. Octopus and FiJi software was subsequently used to process the radiographic images data, to visualize and analyze the crack development and its propagation.

Table 2. Technical parameters of the X-ray CT system XT H 225 ST.

Parameter	Technical data	
Operating voltage and power output of X-ray source	Reflection target	225 kV/225 W
	Reflection rotating target	225 kV/225 W
	Transmission target	180 kV/20 W
X-ray focal size (reflection mode / transmission mode)	<3 μm / <1 μm	
Maximum weight / height / diameter of the scanned samples	50 kg / ca 0.25 m / 0.25 m	
Maximum X-raying mass of the analyzed samples	237 kg/m^2	
X-ray detectors (16-bit contrast resolution)	Flat panel detector PE1611 with dimension of 400 × 400 mm and number of 16 million of pixels (100 μm per pixel)	

2.4. Description of the experiment process

A prepared cylindrical specimen was inserted into the specimen chamber (Fig. 2B) and supported with two cylindrical supports made of carbon fiber composite material. Subsequently, the sample was centered in the chamber and the chamber was closed. The loading device was placed into the X-ray CT inspection system. The conventional cone-beam radiography arrangement was used for scanning. The longitudinal axis of the loading device (direction of loading) was perpendicularly oriented to the axis of the imaging chain (X-ray tube target – object – flat panel detector). The specimen was oriented perpendicularly to the axis of the imaging chain to capture the perpendicular projection of the vicinity of the chevron notch. Focus-object and focus-detector distance were set to capture the region of interest above the notch in the highest possible resolution. The loading device in X-ray setup is shown in Fig. 3. Individual radiographs were obtained during FTT (Fig. 3). During the fracture toughness measurements procedure, the test time, deflection value, and loading force were continuously recorded. Acquisition of

the radiographic images was synchronized with the starting point of the experiment in the time interval of 2 s, and with image exposure of 1 s with two times averaging. Following the FTT, a set of planar X-ray images was visualized using video sequences created from the individual images and analyzed using the methods of digital image processing. Digital image processing covered the following sequential steps: cropping, i.e. determination of ROI (Region of Interest), image radiograph normalization, and radiograph subtraction from the reference image. To highlight the cracks in the subtracted radiographs, a CLAHE (Contrast-Limited Adaptive Histogram Equalization) filter was used.

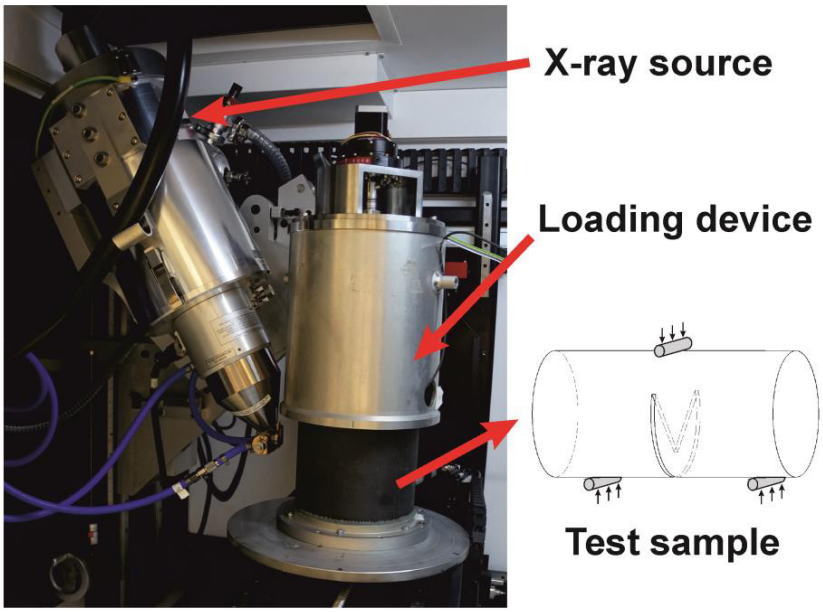

Fig. 3. The scheme of experiment setup used in radiographic measurements.

3. Experiment results and discussion

The measured data from the load cell have been processed into diagrams (see Fig. 4). The diagrams show the time-dependent rock response during specimen loading, adjusted displacement value, and calculated instant increment (or decrease) of loading stated in periodic 2 s time interval. As seen in Fig. 4, the curve depicting the velocity of loading increment per time unit (black curve) is more sensitive and provides better information about the rock response during displacement-driven experiment than the simple time dependence of loading force (red curve). It is obvious that the run of the loading force is not ideally linear in the elastic area of the loading diagram. This behavior is probably influenced by the rock micro-texture (i.e. pore space in rock, quantity and mineralogical composition of matrix as well as rock cement, size, shape and space distribution of clasts, etc.). It is widely known that the internal rock texture affects rock properties, such as bulk density, porosity or strength and deformation properties. The analyses of radiographic images helped to determine the time interval of a recognizable start of the FPZ initiation. This time interval was subsequently plotted into the diagrams presented in Fig. 4. It is clearly visible that the beginning of the crack formation is situated in the area characterized by the change of the progression of the values on the curve characterizing the time dependence of the velocity of loading increment, i.e. in the area of peaks of loading force followed by its subsequent sudden decrease. It can therefore be concluded that this curve could be used as an indicator to determine the FPZ formation. The data presented in Table 3 indicate that the beginning of the crack initiation occurs at the level of ca 80 % of displacement detected at the level of maximum value of measured force (see values marked with the symbol “X” in this table).

Table 3. Loading force and displacement values for the boundaries of the time interval for crack formation in the measured samples.

Sample	Time interval Ti ($t_1 – t_2$) [s]	F_{max} time [s]	Displacement at t_1 [mm]	Displacement at t_2 [mm]	Displacement at F_{max} [mm]	F at t_1 [N]	F at t_2 [N]	F_{max} [N]	X [%]	Y [%]
S2	44 – 48	57.7	217.4	237.4	285.9	312.0	351.0	416.2	80.3	79.6
S4	284 – 288	360.7	283.3	287.3	359.9	319.2	327.8	456.1	79.6	70.9
S5	246 – 250	313.2	245.4	249.4	312.6	344.1	352.3	460.2	79.1	75.6
S6	264 – 268	305.8	263.4	267.4	305.2	372.7	380.6	427.3	87.0	88.1
S7	210 – 214	259.8	209.2	213.2	259.1	335.8	343.8	411.9	82.6	82.4
S13	462 – 466	613.1	230.5	232.5	306.1	341.3	345.9	515.4	76.5	66.7
S14	518 – 522	594.0	258.7	260.7	296.7	450.4	454.6	488.9	87.5	92.5

X – $[(Dt_1 + Dt_2)/2]/D_{Fmax}$, Y – $[(Ft_1 + Ft_2)/2]/F_{max}$, D – displacement, F – loading force

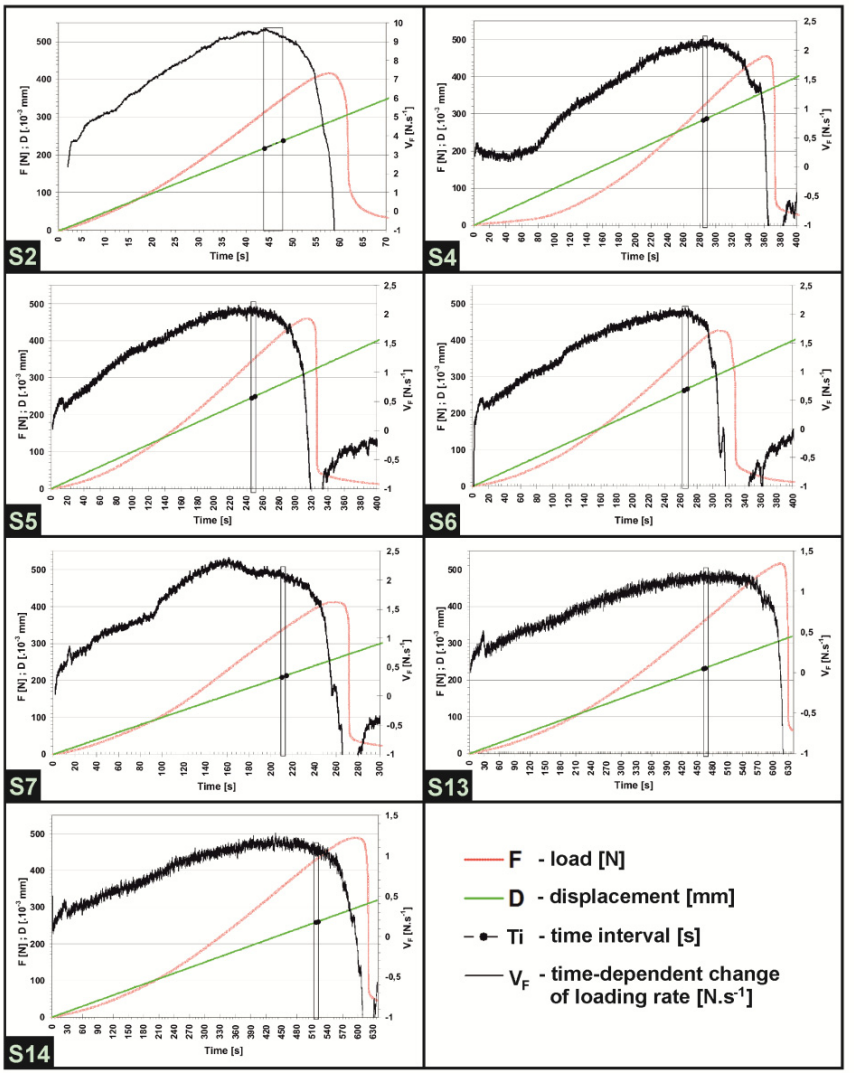

Fig. 4. Experimental curves for CB specimens S2, S4, S5, S6, S7, S13, and S14.

As already mentioned above, in order to determine the beginning of crack formation on each sample under loading, the visual control of the sequence of radiographic images taken in 2 s time intervals was carried out. Subjective designation of a recognizable start of the crack initiation was conducted independently by three different persons. For expression of the moment of crack initiation, the time window (time interval Ti shown in Table 3 as well as in Fig. 4) of 4 s has been selected. This time interval represents two adjacent radiographic images agreed among all observers.

Fig. 5 shows the results of visualization of the crack propagation at different loading steps. The visualization of the crack was obtained by radiograph image subtraction method. The individual images 1–8 demonstrate incremental changes in the internal structure of the selected specimen S4 relative to the reference image (R) obtained in the time of 238 s from the beginning of the specimen loading.

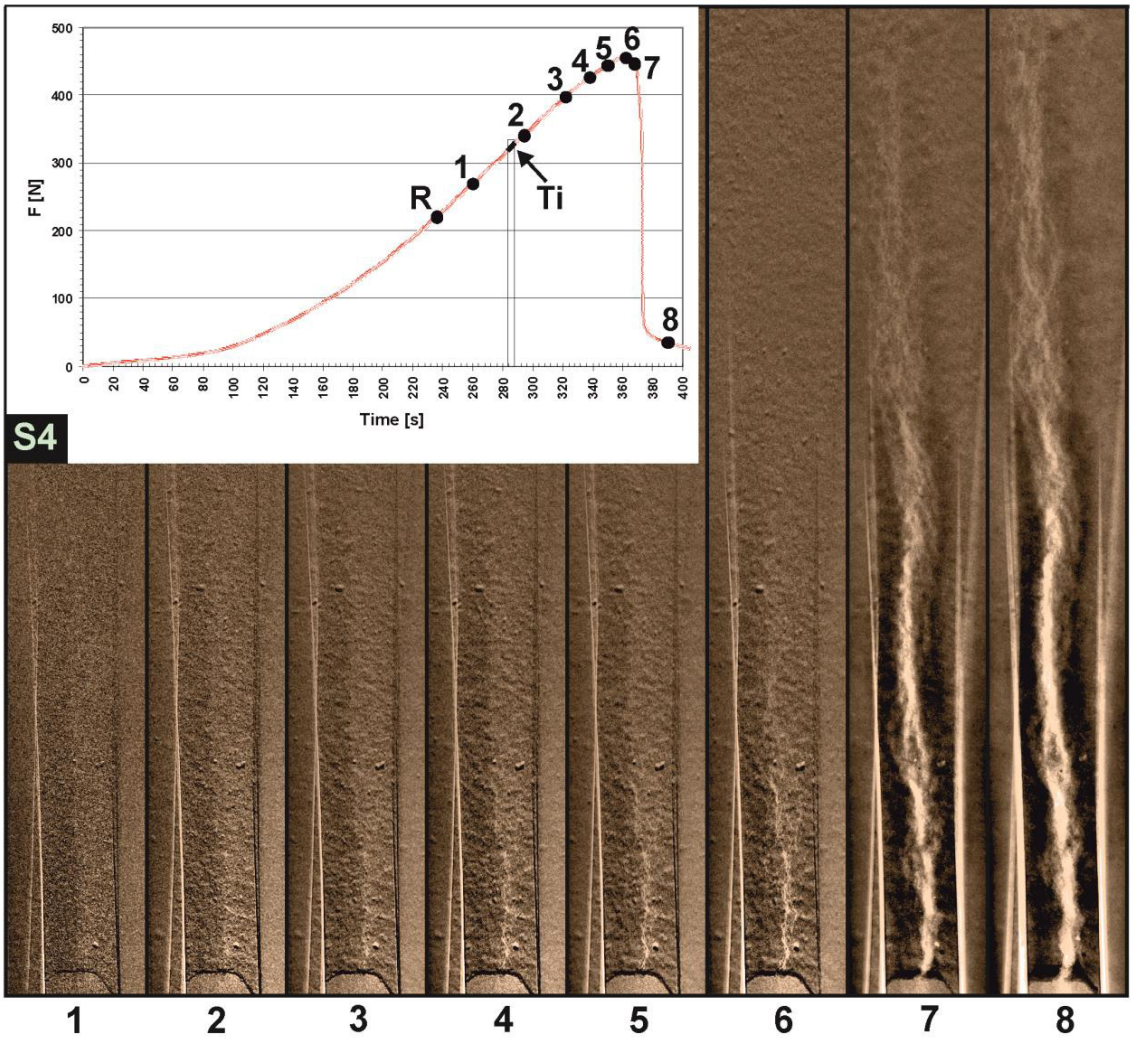

Fig. 5. Series of planar radiographic images at different loading steps (FPZ evolution is clearly visible from the loading step 2).

4. Conclusions

The study carried out on the samples of glauconitic Godula sandstone demonstrates that the joint analysis of radiographic images and Mode I FTT measurement data obtained during the sample loading allows for identification of crack initiation and propagation during displacement-driven loading of the rock specimens. From the preliminary results of the laboratory research, the following conclusions can be drawn.

(1) The starting point of the crack evolution may be situated within the area characterized by the change in the trend of the values on the loading rate changes vs. time (V_F–t) curve, i.e. in the area of maximum values of loading rate with its subsequent sudden decrease.
(2) In the case of the sandstone under study, the crack begins to propagate from the moment when ca. 80 % of the specimen displacement measured at maximum loading force is achieved (see the values marked with the symbol "X" in Table 3).
(3) The V_F–t curve can serve as a useful tool to determine crack initiation (especially after elimination of support setting).

The above-mentioned findings will need to be verified on other basic petrographic types of rocks with different internal structures analyzed using tomographic data acquired from the specimen area predestined to crack propagation. In order to verify the research outcomes, a broader spectrum of different loading rates during displacement-driven loading of rock specimens is recommended. In the case of the sandstone under study, however, it appears that the X-ray computed radiography represents an appropriate method to study the FPZ evolution process.

Acknowledgements

The research was supported by Project LO1406 of the Institute of Clean Technologies for Mining and Utilization of Raw Materials for Energy Use under the National Sustainability Program I (2013–2020), by the Czech Republic Project for the long-term conceptual development of research organizations (RVO: 68145535), and by the projects GA16-18702S (AMIRI) and GA15-07210S of the Czech Science Foundation and also by the project RINGEN+, reg. no. CZ.02.1.01/0.0/0.0/16_013/0001792 supported by Research, Development and Education Operational Programme.

References

[1] A. Fakhimi, A. Tarokh, Process zone and size effect in fracture testing of rock, Int. J. Rock. Mech. Min. Sci. 60 (2013) 95–102.
[2] P. Frantík, V. Veselý, Z. Keršner, Parallelization of lattice modelling for estimation of fracture process zone extent in cementitious composites, Adv. Eng. Softw. 60–61 (2013) 48–57.
[3] S. Das, M. Aguayo, G. Sant, B. Mobasher, N. Neithalath, Fracture process zone and tensile behavior of blended binders containing limestone powder, Cem. Concr. Res. 73 (2015) 51–62.
[4] M.D. Wei, F. Dai, N.W. Xu, T. Zhao, K.W. Xia, Experimental and numerical study on the fracture process zone and fracture toughness determination for ISRM-suggested semi-circular bend rock specimen, Eng. Fract. Mech. 154 (2016) 43–56.
[5] M. Ghamgosar, N. Erarslan, Experimental and numerical studies on development of fracture process zone (FPZ) in rocks under cyclic and static loadings, Rock Mech. and Rock Eng. 49 (2016) 893–908.
[6] A. Fakhimi, F. Wan, Discrete element modeling of the process zone shape in mode I fracture at peak load and in post-peak regime, Int. J. Rock Mech. Min. Sci. 85 (2016) 119–128.
[7] W. Chengyong, L. Peide, H. Rongsheng, S. Xiutang, Study of the fracture process zone in rock by laser speckle interferometry, Int. J. Rock Mech. Min. Sci. & Geomech. Abstr. 27 (1990) 65–69.
[8] I. Kumpová, T. Fíla, D. Vavřík, Z. Keršner, X-ray dynamic observation of the evolution of the fracture process zone in a quasi-brittle specimen, J. Instrum. 10 (2015) 1–8.
[9] M. Vavro, L. Vavro, P. Martinec, K. Souček, Properties, durability and use of glauconitic Godula sandstones: a relatively less known building stone of the Czech Republic and Poland, Environ. Earth Sci. 75 (2016) 1437.
[10] L. Vavro, Fracture toughness of rock and its determination for geomechanical assessment of rock and rock mass, Ph.D. dissertation, VŠB-Technical University of Ostrava, Czech Republic, 2014 [in Czech].